Teleseismic deep sounding of the velocity structure beneath the Rio Grande rift

P. M. Davis, E. C. Parker, J. R. Evans, H. M. Iyer, and K. H. Olsen
1984, pp. 29-38. https://doi.org/10.56577/FFC-35.29

in:

Rio Grande Rift (Northern New Mexico), Baldridge, W. S.; Dickerson, P. W.; Riecker, R. E.; Zidek, J.; [eds.], New Mexico Geological Society 35th Annual Fall Field Conference Guidebook, 379 p. https://doi.org/10.56577/FFC-35

This page is intentionally left blank to maintain order of facing pages.

TELESEISMIC DEEP SOUNDING OF THE VELOCITY STRUCTURE BENEATH THE RIO GRANDE RIFT

P. M. DAVIS', E. C. PARKER', J. R. EVANS', H. M. [YEW, and K. H. OLSEN'
'Department of Earth and Space Sciences, University of California at Los Angeles, Los Angeles, California 90024; 'U.S. Geological Survey, Menlo Park, California 94025;
3Institute of Geophysics and Planetary Physics, Los Alamos National Labortory, Los Alamos, New Mexico 87545

INTRODUCTION

A 1,000-km-long linear array of 20 seismic stations between Moab, Utah, and Odessa. Texas, crossing the Rio Grande rift near Santa Fe, recorded 40 useful teleseisms during December 1982 and January 1983. The orientation of this array was chosen to be at an angle of 45° to the strike of the rift because teleseismic arrivals commonly occur along this azimuth. P-wave arrival times show a clear delay of as much as 1.5 sec centered on the rift with measurable delays extending several hundred kilometers to either side of it. This delay pattern correlates well with the broad negative Bouguer gravity anomaly in this area which is in isostatic compensation with the topographic uplift. Variation in crustal velocities is too small to fully explain the delay pattern. Preliminary inversions of the data require a low-velocity, low-density body situated well below the Moho. Constraining it to lie completely within the crust significantly degrades the fit of the model to the data and rules out an Airy type of isostatic compensation. Both a damped-least-squares block inversion and fitting of a bowed "lithosphere—asthenosphere interface" to the data indicate a rift-centered delaying structure at upper-mantle depths (70-200 km), at least 500 km wide. We compare velocity, gravity, and topography across the rift.

The Rio Grande rift, which separates the Great Plains to the east from the Colorado Plateau and Basin and Range province in the west, lies just to the east of the continental divide in a region of broad uplift, high heat flow, and low gravity. Figure 1 (from Cordell, 1978) illustrates the topographic uplift and regional gravity low extending from the Colorado Plateau into the Great Plains. This profile and several similar ones at 10 intervals lying between 33° and 37°N latitude, suggest that a broad, linear low-density zone several hundred kilometers wide is associated with the uplift, and has given rise to the rift, a low-lying block (some 50 km wide). Ander (1980) has presented a wide range of gravity models which fit the observations. We have used the teleseismic P-wave delay technique to provide extra constraints on the models in order to better identify the position and shape of low-density zone.

Spence et al. (1982) reported differential travel times of 0.6 sec between within-rift stations of a northern New Mexico seismic net. This pattern was interpreted as due to a deep-seated, low-velocity body beneath the Valles caldera. They also reported a northeast-trending, low-velocity zone aligned in the same direction as the Jemez lineament. Superimposed on this pattern was up to a 1.8 sec difference between the rift stations and the distant WWSSN station at Lubbock, Texas. Our experiment was designed to investigate this larger, longer-wavelength anomaly, which necessarily required installation of stations over a much longer baselength than that covered by the northern New Mexico net.

THE EXPERIMENTAL METHOD

Geophysical methods to investigate localized velocity heterogeneity near the base of the lithosphere are limited. Surface waves which are generally used to determine lithospheric thickness are difficult to interpret where the structure is not approximately plane-layered. Structure lying beneath the Moho is too deep for economically feasible conventional refraction and reflection studies. Teleseismic deep sounding represents the most practical method. The P-wave-delay technique is well developed and has been used to search for magma chambers and deep structures in diverse tectonic environments. However, this is the first linear transect of a major rift. Descriptions of the technique can be found in papers by Aki (1982), lyer (1975, 1984), lyer et al. (1981), Evans (1982), and Sharp et al. (1980). Briefly, the method consists of timing arrivals from distant earthquakes and subtracting from them arrival times for laterally homogeneous earth. Any residuals remaining are attributed to lateral heterogeneity beneath the seismic array, since distant heterogeneities such as those at the source will smear out due to geometric spreading. Angles of incidence and azimuth are calculated from source parameters using a standard earth model. The pattern of residuals has been observed to shift in response to different angles of incidence and azimuth of the incoming waves. Given enough rays at different angles, the data can be inverted to determine velocity at depths of up to about half the array dimension, with a resolution equal to station spacing near the surface but decreasing with depth.

THE EXPERIMENT

Figure 2 shows the 20 recording-station locations along a 1,000-km line for the (joint UCLA, USGS, LANL) 82/83 experiment. A NW—SE orientation was used since teleseismic arrivals lie predominantly along this azimuth so that rays from the NW and SE intersect in regions lying beneath the array. This geometry was important for our initial line to avoid ambiguity in the inversion of the data. Otherwise we must

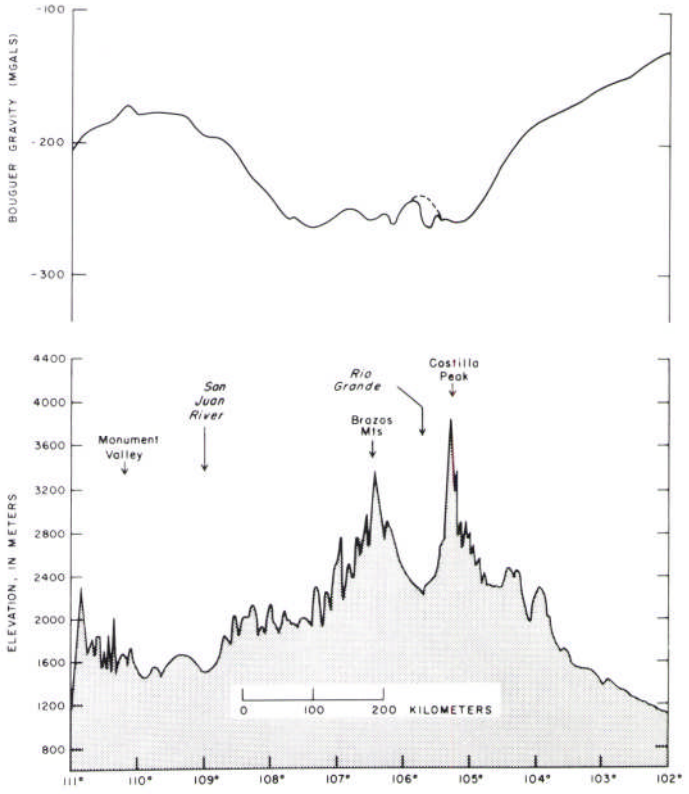

FIGURE 1. E–W gravity profile across the Rio Grande rift at latitude 37°N (from Cordell, 1978).

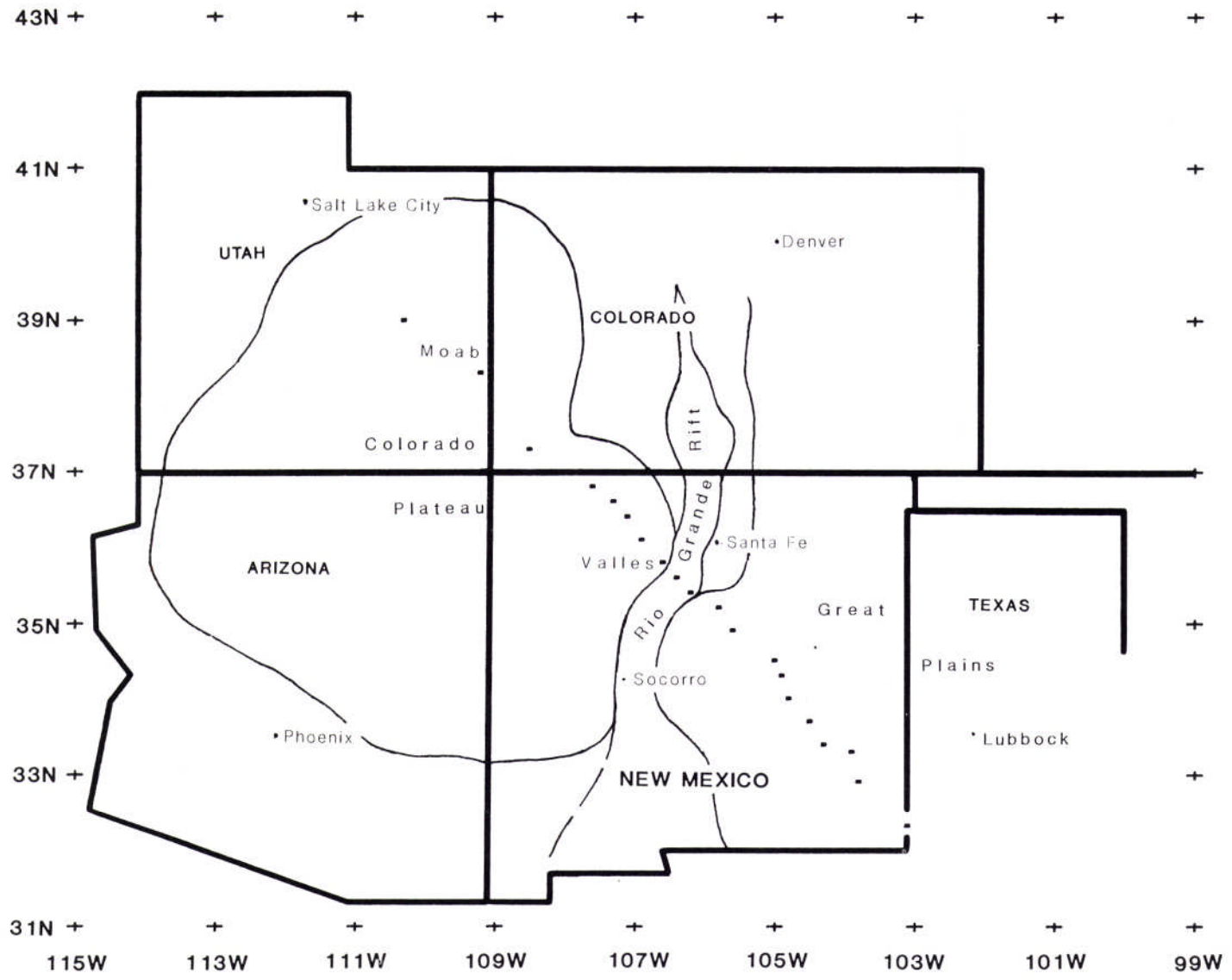

FIGURE 2. Location map of portable seismic recording stations used in this experiment.

assume that the structure is two-dimensional. The array ran from late November 1982 until late January 1983. Field base stations were set up at Moab, Utah, and Santa Fe and Roswell, New Mexico. Field parties, comprised of two people and a 4-W/D vehicle, serviced six instruments over 300-km section of line. This involved synchronizing time, changing tapes and batteries every five days at each site, as well as data playback and instrument repair, resulting in a full schedule. Typical driven distances per vehicle amounted to 10,0(X) miles.

Figure 3 is a sample of the data for a teleseism from Honshu. The relative P-wave arrival times can be measured to 0.1 sec. Residuals are found by subtracting from the arrival times computed travel times listed in the Herrin tables. Relative residuals are formed for each event by subtracting the mean residual from the raw residuals.

Of the 60 earthquakes recorded, 40 are of sufficient signal-to-noise ratio to be used in an inversion. Twenty-five of these lie along the array azimuth. For graphical purposes we have grouped these 25 into two groups of delta (epicentral distance) greater than or less than 50°. The groups are further subdivided and averaged to give residuals from the NW and SE. These four curves are shown in Figure 4a, 13-4a shows averaged teleseismic residuals for delta greater than 50°, steep incidence, and 4b shows these for delta less than 50°, shallow incidence. In both cases the patterns shift in response to the reversal in azimuthal incidence. For the shallower incidence the shift is greater. Modeling this shift with a simple spherical-velocity anomaly places it at a depth of 100 km.

INTERPRETATION

Interpretation of the residual pattern requires additional assumptions to give a unique result. Consider the data plotted in Figure 4a, b. We assume that the regional shifting pattern is mainly due to upwarp of the asthenosphere–lithosphere boundary (which we define as the boundary at the base of the lithosphere separating high P-wave and S-wave velocities from lower values in the low-velocity zone of the asthenosphere); that localized hetergeneity gives rise to the small-scale variations. We can test how to invert for such a boundary using synthetic models. We computed and inverted data from a synthetic model which gave similar residual patterns for the range of incident angles and azimuths of our experimental data set in two ways: (1) downward projection of the data to give the boundary shape directly as outlined below, and (2) the two-dimensional (Aki et al., 1977) damped-least-squares block method as implemented by Ellsworth (1977). The first method gives an exact result; the second smeared the negative velocity perturbation at depth to shallow depths. This occurs because of the limited range of incidence angles, I less than 38°; therefore, the depth resolution is poor—e.g., parts of the residual patterns for I = 38° that overlap are independent of incidence and can equally be placed at

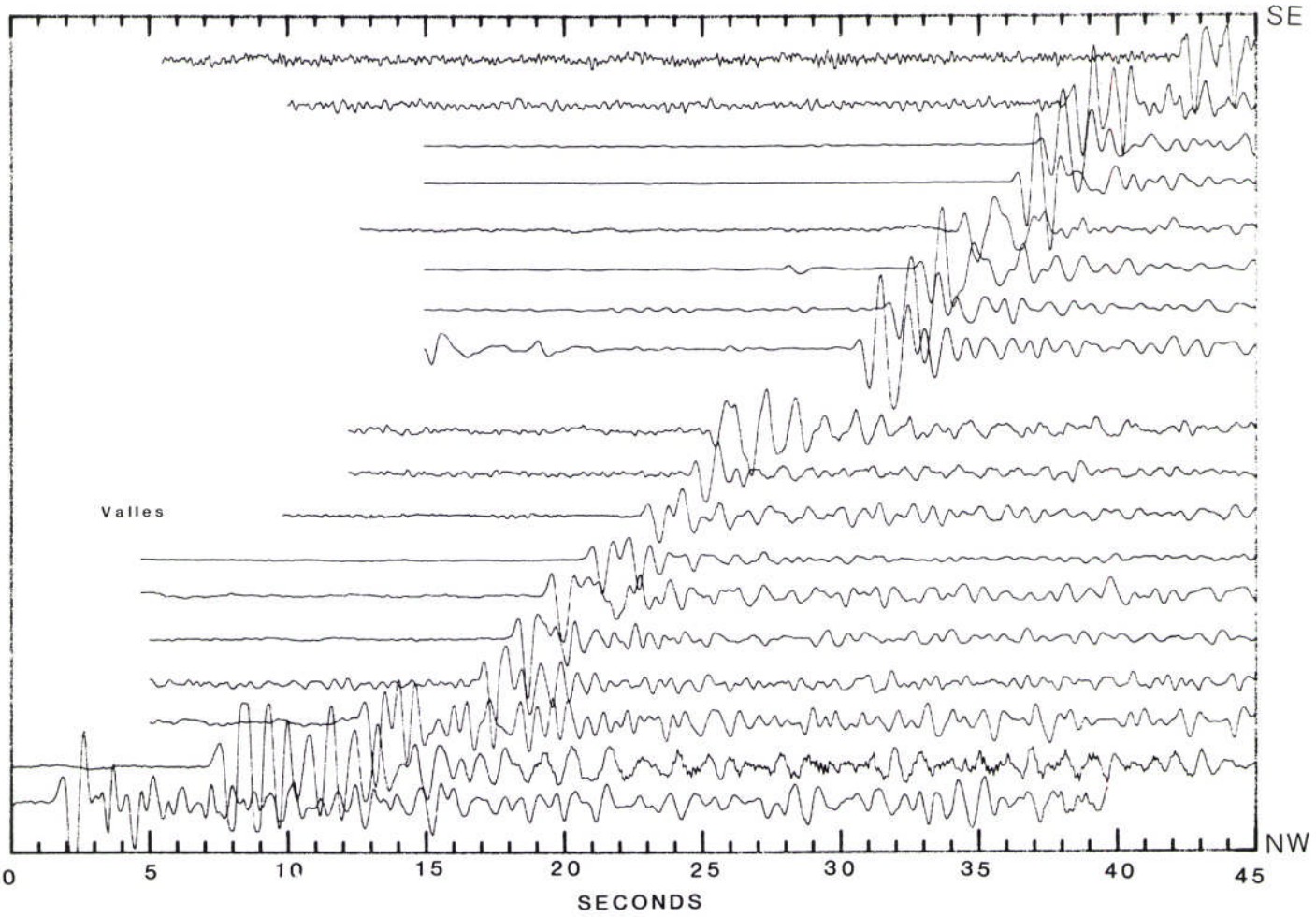

FIGURE 3. Record section of arrivals from Honshu earthquake of 15 January 1983 showing that timing to 0.1 sec is feasible for this signal-to-noise ratio.

either deep or shallow depth in the crust. The least-squares solution favors neither and smears this part of the solution over the whole depth range.

The first method of downward projection is justified on the grounds that it achieves the simplest and smoothest geological model and requires a minimum number of parameters (i.e., 7) in the inversion.

DOWNWARD PROJECTION OF TELESEISMIC RESIDUALS TO SOLVE FOR A VELOCITY INTERFACE

We assume that the long-wavelength teleseismic anomaly found on our profile across the Rio Grande rift is due to a single velocity interface—the lithosphere–asthenosphere transition which upwarps beneath the rift and has a north–south strike, i.e., parallel to the rift. Figure 5 shows our analysis method. If the interface is not too deep and velocity contrasts not too extreme, a straight ray and plane wave approximation for the teleseismic waves is adequate. The raw residuals will then be proportional to the length of the ray in the anomalous velocity zone. The raw residual pattern gives a distorted picture of the interface, i.e., it is projected onto a rotated axis. Since we know the angle of incidence, we can transform the projection and regain the original shape (dotted curves in Figure 5).

The ith ray length h, in low-velocity material is

$$h,' = V,V,t,/V,–V,$$
$$= A\ t, \text{ at positions } xo,' \text{ on the surface}$$

where to is the ith residual, V, and V, are upper and lower velocities, respectively, and A is a parameter given by the fit. The transformation to give the interface geometry is

$$h, = h,' \cos I$$
$$= x,' + h,' \sin 1 \quad (1)$$

where I is the angle of incidence for a given event. If the depth is D, the true lateral position of the anomaly is given by

$$x, = x," – D \tan I \quad (2)$$

Relative residuals corresponding to 22 earthquakes (Table 1) arriving from either the NW or SE, i.e., along our 1,000-km line of stations, are shown in Figure 6. Raw residuals for each event have been demeaned to form relative residuals. Transformations (1) and (2) were applied to the data and parameters A and D varied until the sum of squares of residuals to a sixth-order polynomial fit was minimized. The minimum is fairly broad. The range of acceptable models is shown in Table 2. Figure 7 shows the best-fit model. Table I lists acceptable-alternative models lying in a range given by the criterion (Jenkins and Watts, 1968) that S is less than

$$S_{,} (1 + m/n–m\ f(m, n–m, (I – a)))$$

where n is the number of data, m the number of parameters, f the value of the F-statistic for confidence limit a with m, and n–m degrees of freedom. S is the sum of squares of residual differences for a particular model, and S,, is the sum of squares of residuals for the best-fitting model. If we take V, = 8 km/sec, the velocity contrast for our chosen model is 8%.

Values of the parameters used to contrain acceptable models of Table 2 were m = 7, n = 270, a = 95%. The average misfit of the polynomial model to the data was 0.3 sec. The best-fit model has a mean depth of 140 km and A = 80 km/sec.

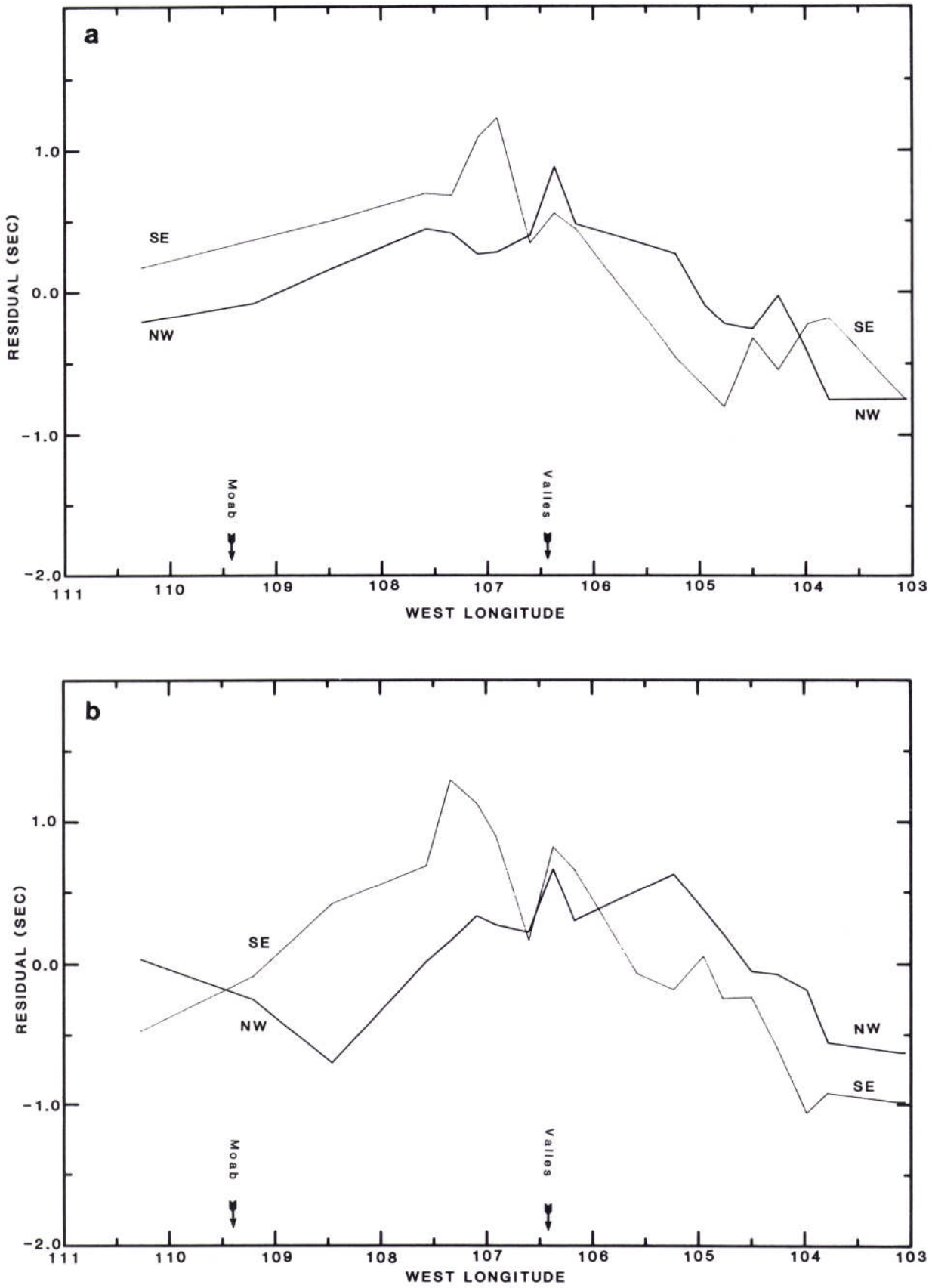

FIGURE 4. **a,** Teleseismic residuals for delta greater than 50°. SE curve is the average of two events from the southeast. NW curve is the average of seven events from the northwest. **b,** Teleseismic residuals for delta less than 50°. SE curve is the average of six events from the southeast. NW curve is the average of ten events from the northwest. Shifts in the curves of a and b, which are dependent on azimuth and incident angle of arrival, indicate an anomaly depth of at least 100 km.

TABLE 1a. Station locations. Each station consists of a 1 Hz, L4C vertical seismometer and recorder.

sta	latitude	longitude	elevation
RG1A	32 19.35	103 3.81	1013.
RG1S	32 19.35	103 3.81	1013.
RG2A	32 57.42	103 46.61	1323.
RG2S	32 57.42	103 46.61	1323.
RG3A	33 18.94	103 58.51	1173.
RG4A	33 28.87	104 15.33	1187.
RG5S	33 43.66	104 30.03	1247.
RG6A	34 2.62	104 46.33	1443.
RG7A	34 17.53	104 57.30	1641.
RG8A	34 30.73	105 13.51	1768.
RG8S	34 30.73	105 13.51	1768.
RG9A	34 52.42	105 35.03	2080.
RG9S	34 52.42	105 35.03	2080.
RGAA	35 13.40	105 49.08	2100.
RGAS	35 13.40	105 49.08	2100.
RGBS	35 24.25	106 10.06	2006.
RGCS	35 37.24	106 22.16	1652.
RGDS	35 48.66	106 36.04	2408.
RGES	36 9.70	106 54.46	2502.
RGFS	36 24.96	107 5.19	2262.
RGGS	36 35.00	107 20.51	2246.
RGHS	36 47.45	107 34.41	2086.
RGJS	37 16.38	108 27.61	2554.
RGLS	38 20.65	109 12.44	2359.
RGMS	39 .34	110 15.94	1311.

TABLE 1b. Hypocentral coordinates of earthquakes used in the inversion.

No.	Event	Time	(UT)	Longitude		Latitude		Depth	Place
01	82 358	03 49	52.7	94.543	W	15.304	N	57	OAXACA
05	82 363	07 02	31.4	139.336	E	33.763	N	19	HONSHU
06	82 363	11 06	25.8	91.603	W	14.405	N	85	GUATMALA
07	82 363	12 17	46.1	139.333	E	33.732	N	26	HONSHU
10	82 365	01 35	35.2	68.046	W	21.386	S	130	CHILE
11	82 365	02 46	50.7	78.962	W	10.743	S	28	PERU
12	82 365	03 47	28.5	68.464	W	20.993	S	118	CHILE
16	83 001	05 31	56.1	69.114	W	16.943	S	172	PERU/BOL
17	83 001	11 18	07.7	147.174	W	61.336	N	55	ALASKA
77	83 006	12 29	48.6	148.120	E	44.543	N	66	KURILS
78	83 009	10 42	47.7	163.125	E	55.163	N	33	KAMCHTKA
79	83 009	21 03	54.2	163.244	E	55.179	N	33	KAMCHTKA
34	83 010	09 17	34.7	68.470	W	22.006	S	121	CHILE
35	83 010	12 32	21.6	63.301	W	27.237	S	558	ARGENTIN
39	83 014	18 20	52.6	154.154	W	55.911	N	33	KODIAK
40	83 015	00 39	34.2	136.040	E	33.268	N	435	HONSHU
41	83 015	00 49	53.6	160.076	E	52.844	N	30	KAMCHTKA
50	83 018	07 44	28.6	88.817	W	12.930	N	70	CENTAMER
80	83 021	10 25	53.5	142.988	E	42.422	N	76	JAPAN
57	83 023	14 29	28.5	77.543	W	6.485	N	9	COLOMBIA
62	83 026	01 05	50.7	66.997	W	23.971	S	186	CHEL/ARG
65	83 027	19 01	35.3	66.960	W	24.105	S	188	CHI/ARGN

TABLE 2. Sum of squares of residuals, SSQ, as a function of $A = V_2V_1/V_1-V_2$, and depth, D, for the projection model inversion. Acceptable models are denoted by asterisks.

Depth	40	90	140	200	250	300	350
A							
40	25.7	23.6	22.5*	23.0*	25.8	29.5	34.0
80	25.4	23.4	22.3*	23.1	25.3	28.8	33.1
120	25.3	23.5	22.6*	23.0*	25.4	28.6	32.5
160	25.4	23.6	23.1	23.8	25.7	28.6	32.2
200	25.5	24.3	23.8	23.8	26.0	28.6	32.5

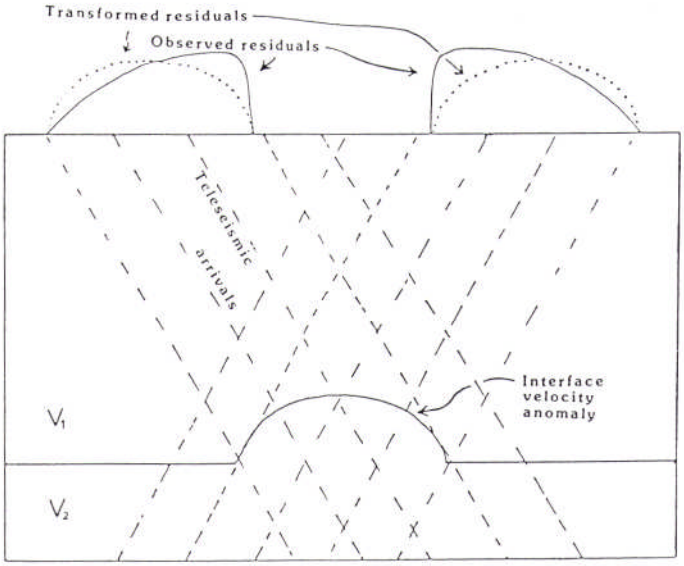

FIGURE 5. Cartoon showing downward-projection method of inverting teleseismic residuals to find the shape of a velocity interface.

DAMPED-LEAST-SQUARES TWO-DIMENSIONAL BLOCK MODEL

Relative residuals were inverted to determine percent velocity perturbations about average layer velocities following the approach of Evans (1982). No earth-flattening transform was used since our final model geometry, 1,000 km x 200 km, was of the same order as those tested by Evans (1982), who found earth-curvature effects to be of second-order importance. The blocks were aligned north—south, roughly parallel to the strike of the rift.

We ran a series of tests to determine the uniqueness and minimum parameterization of the block model and, having determined an optimal model, tested the hypothesis that all the residuals are due to slowness in the crust or upper lithosphere rather than in the deep lithosphere. The hypothesis was rejected at the 99.9% confidence level. The data require a deep, low-velocity zone.

Since our station spacing ranged from 30 to 140 km, we chose a block width of 100 km. Unperturbed crustal and upper-mantle velocities were set at 6.5 and 8.0 km/sec, respectively, with the transition at a depth of 40 km. We then varied the number of layers (from six down to our final value of three), the positions of the interfaces between layers, and the total depth of the model. Since the number of layers determines the number of parameters, for any given model depth we were able to arrive at an optimum number of layers, three by means of the F-test. However, non-uniqueness became a problem when comparing different interface depths. Models with an overall depth of 500 km were found to have a fit negligibly different from those of 200-km depth (average misfit 0.285 sec cf. 0.297 sec). Although the velocity variation was qualitatively similar, its amplitude was proportionately reduced in the deeper model. Also, placing the second interface at 70 km (misfit 0.297 sec) was not significantly different from placing it at

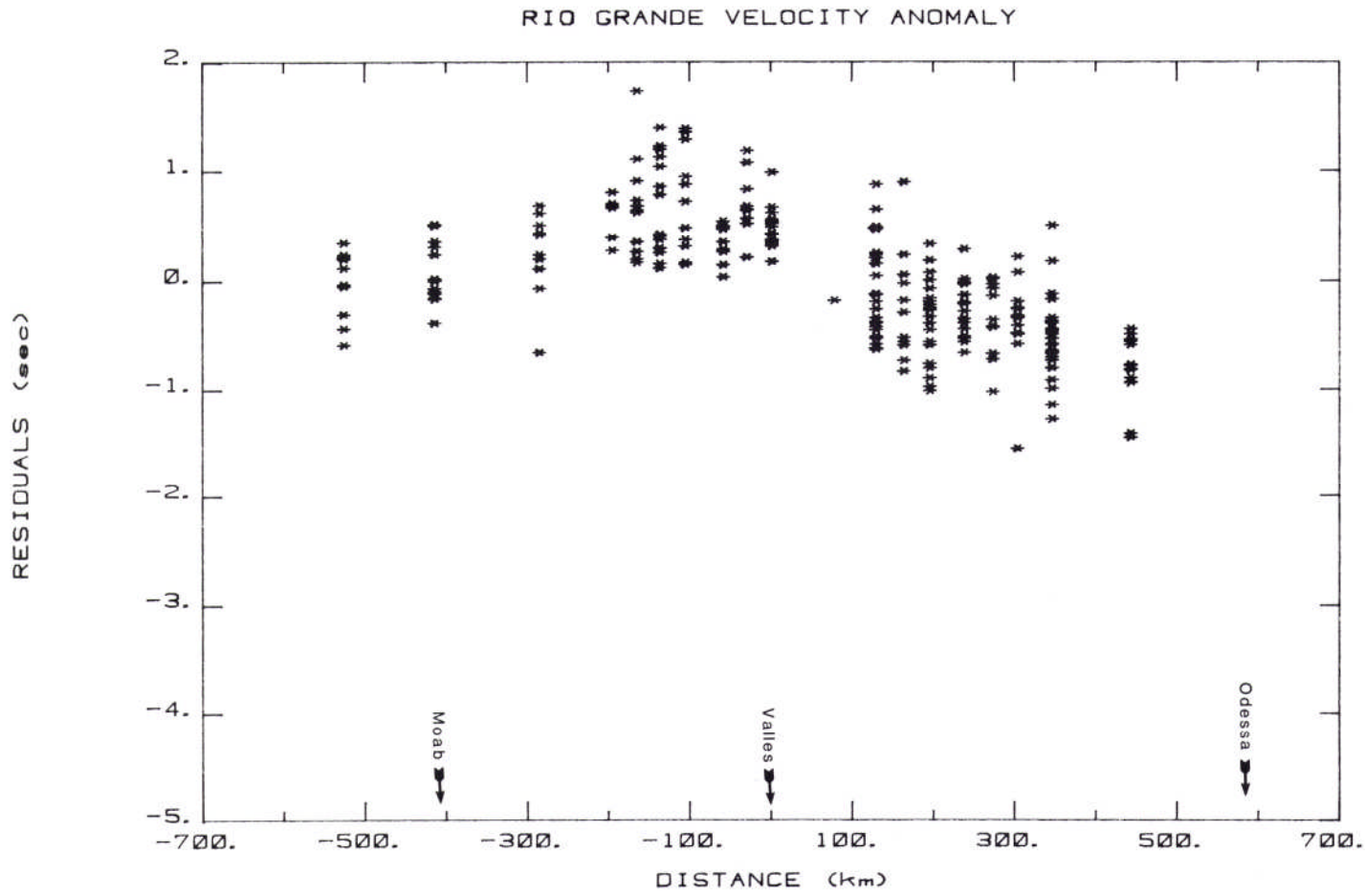

FIGURE 6. Teleseismic residuals from 22 earthquakes measured on stations spanning the Rio Grande rift.

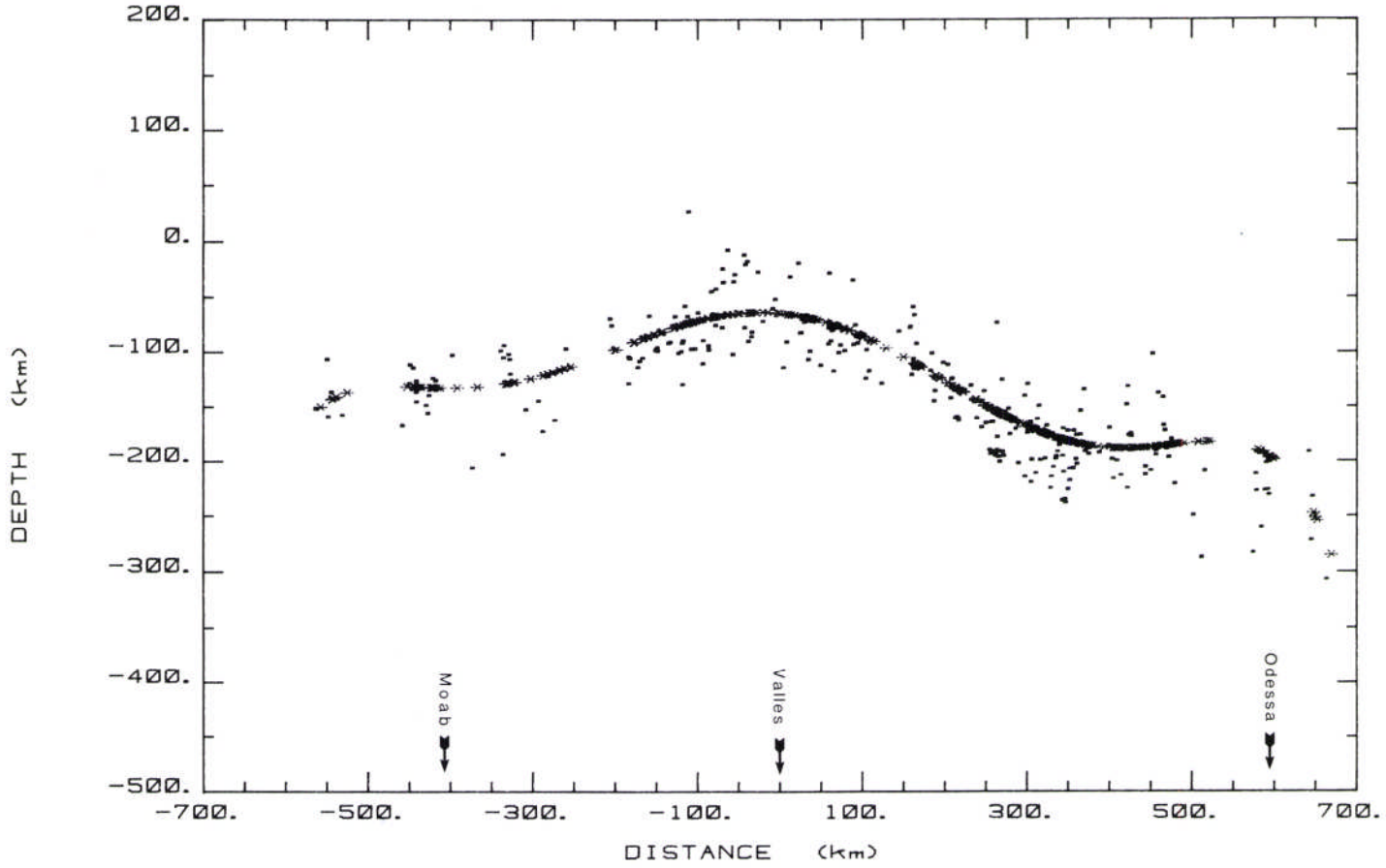

FIGURE 7. Results of downward-projection modeling of the residuals. The best fitting polynomial is in asterisks.

150 km (misfit 0.300 sec). Therefore, the model we present in Figure 8 was chosen from this non-unique set because its interfaces correspond to those of the polynomial model of the previous section, that is a 40-km crust, a 70-km upper and 200-km lower boundary of a low-velocity body. The main feature of this model is a 5% reduction in velocity in the lowest center-most block, beneath the Valles caldera, with coherent negative variation on either side. Smaller variations in the upper two layers are incoherent. Standard errors given by the least-squares solution are all about 0.6%. The diagonal elements of the resolution matrix ranged from 0.55 in the top layer to 0.86 in the lowest layer.

The percent reduction in variance after subtracting model values from the data was 71%. This model is in reasonable agreement with the polynomial model (Fig. 7). The velocity contrast of 6% is slightly less than the 8% found in that case, but this may be due to the smearing effect mentioned earlier. To test the hypothesis that the source of the relative residuals lies no deeper than the crust, we confined the block model to the upper 40 km, keeping the number of blocks constant. The variance reduction was only 50% compared with 71% for the deeper models. Comparison with F-statistic values rejects this hypothesis with greater than 99.9% confidence.

COMPARISON WITH BOUGUER GRAVITY

The Bouguer gravity anomaly calculated for both the polynomial model and the block model fit the measured data for the area well.

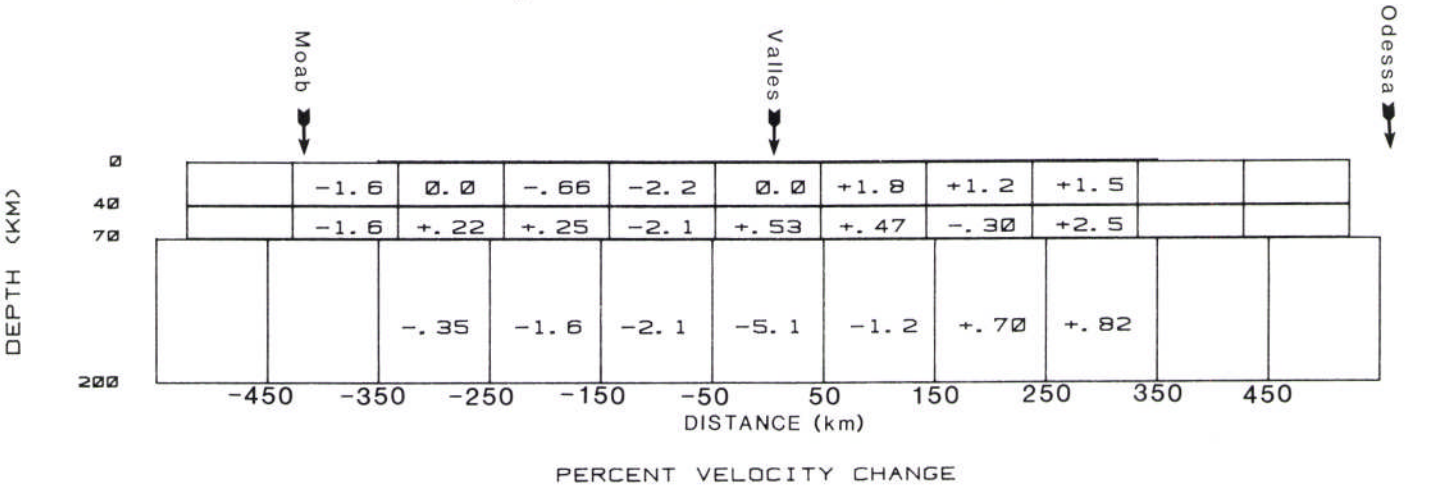

FIGURE 8. Results of two-dimensional block modeling of the residuals. The numbers represent percent change in velocity relative to starting model velocities.

Figure 9 shows the fit for the gravity from the polynomial model for which the adjusted density contrast in the low-velocity zone gave a value of —0.05 gm/cc. This is a much smaller contrast than that calculated from the Nafe—Drake relationship (0.16 gm/cc). However, we are not in a position to pursue the implications here.

The shape of the topography is also somewhat in agreement with topography in isostatic balance with the polynomial model. However, this requires a lower density contrast (— 0.03 gm/cc), and we have not yet reconciled these two values.

PREVIOUS LOCAL SEISMIC STUDIES

Previous seismic work has been concentrated within the rift zone. Figure 1 shows a positive gravity anomaly centered on the rift and superimposed on the regional gravity low. The smaller-scale anomaly is thought to be due to a combination of mantle upwarp into the base of the crust and crustal thinning due to tectonic extension (Cordell, 1978). However, broad-scale igneous intrusion of the shallow crust represents another possibility. Support for the mantle-upwelling hypothesis is seen in the seismologically determined crustal thicknesses as summarized by Olsen et al. (1979), in which the depth to the base of the rift crust (33 km) is shown to be 12 and 17 km shallower than for the Colorado Plateau (45 km) and Great Plains (50 km), respectively. Corroborating evidence comes from Keller et al. (1979), who combine surface-wave dispersion measurements and refraction data to infer a similar structure with the rift Moho at a depth of 35 km, as well as from the tentative identification of a Moho reflector at 12 sec on the COCORP line (Brown et al., 1979), which translates to a depth of 35 km. In contrast, Phinney (1964) used the spectral-ratio method to find a Moho depth of 35-40 km on the rift beneath the WWSSN station at Albuquerque. The high value of this result may be a consequence of allowing both depth and velocity to vary during modeling (Olsen et al., 1979).

One of the most striking seismic results seen on the rift in the vicinity of Socorro is the evidence for the existence of a 19-km-deep crustal magma layer (Sanford and Long, 1965; Sanford et al., 1973; Rinehart et al., 1979; Rinehart and Sanford, 1981) confirmed by the COCORP line (Oliver and Kaufman, 1976; Brown et al., 1979). Evidence that it might be a widespread phenomenon beneath the rift is seen in the study of the amplitudes of arrivals from the refraction experiment of Olsen et al. (1979), who infer a layer thickness of a few km.

Other seismological evidence as to the nature of the rifting includes the observation of low P, velocities of 7.6 km in the upper mantle beneath the rift (Olsen et al., 1979) compared to 7.8 km/sec beneath the Colorado Plateau and 8.2 km/sec beneath the Great Plains. Crustal thinning and low P_n velocity have been observed in other rift zones, e.g., the Rhinegraben (Giese et al., 1976), the East African rift (Long et al., 1973), and the North Sea (Christie and Sclater, 1980). However, a recent study of Murdock and Jacksha (1981) finds a normal P. velocity of 8.0 km/sec beneath the Rio Grande rift, excluding the possibility of a wide zone of asthenospheric intrusion at the base of the crust.

Tracing rays through these crustal structures gives rise to a long-wavelength lateral variation no greater than 0.2 sec, providing further evidence that the delaying structure lies at depth in the mantle. Smaller-scale variations of 0.5 sec have been seen corresponding to deep sedimentary basins.

REGIONAL SEISMIC STUDIES

Our approach to modeling the residuals has been to build on what is already known of the lithosphere/asthenosphere structures in the region by incorporation of the delay model. Biswas and Knopoff (1974) examined Rayleigh-wave dispersion along a number of paths across the United States and found significant regional variations in S-wave velocities in various subregions of the continent. The south-central part of the continent and the Basin and Range are characterized by a well-

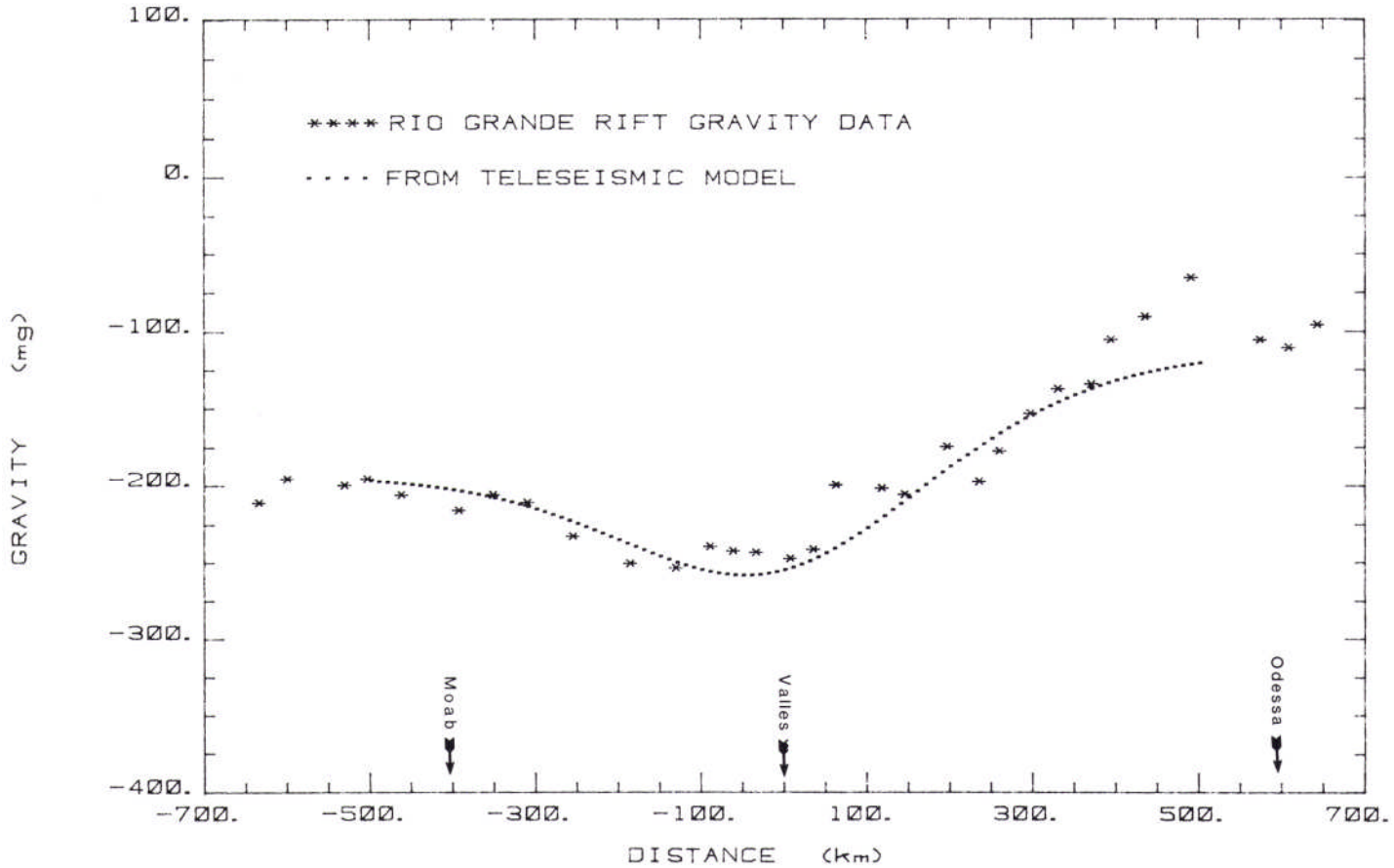

FIGURE 9. Gravity anomaly measured along teleseismic array compared to gravity calculated from polynomial of Figure 5.

developed low-velocity channel (LVZ) for S waves in the upper mantle. The north-central United States has high upper-mantle S-wave velocities without the development of a significant low-velocity channel. They presented a suite of models for a path (GOL—DUG) lying just to the northwest of our array and a path (SHA—LUB) lying to the southeast. They find a lid thickness of 35-95 km underlying a 48-km crust with lid (shear-wave) velocities around 4.6 km/sec and low channel velocities around 4.3 km/sec, i.e., a lithospheric thickness (lid plus crust) in the range of 83-145 km. The maximum lithospheric thickness interfaces to the shallowest polynomial boundary (Fig. 7) in the west. The eastern boundary lies somewhat deeper, 190 km; the western side lies at a depth of 130 km.

Further to the west, in the Basin and Range province, Biswas and Knopoff (1974) found a well-developed low-velocity channel with S-wave velocity in the range of 4.1-4.3 km/sec. More recent studies (Priestley and Brune, 1978; Priestley et al., 1980) of the Great Basin of Nevada and western Utah show 65-km-thick crust and lid (35-km crust and 29-km lid), with the lid-LVZ-velocity contrast 4.5 km/sec to 4.05-4.12 km/sec. The central part of our polynomial fit (Fig. 7), which lies beneath the rift at 75-km depth, is not very different from the Great Basin lithospheric thickness. However, although the polynomial fit of Figure 7 shows a degree of agreement with structures determined from Rayleigh waves, there are some remaining points to be resolved. Where P-wave velocities have been associated with low S-wave velocities (Priestley et al., 1980; Dziewonski et al., 1975; Burdick and Helmberger, 1978) in the LVZ, the percent reduction in P velocity is about half of that in S velocity. Our model reduction in P velocity is 8%, implying an unprecedented reduction of 14% in S velocity. Also, the LVZ has been associated with increased density values (Biswas and Knopoff, 1984; Dziewonski et al., 1975), which is opposite to our conclusion. We can trade off less P-wave-velocity perturbation with increased amplitude of the polynomial variation. However, this would place the flanks unacceptably deep to interface with the surface-wave models. It therefore appears that if we invoke asthenospheric upwarp to explain the gravity, topography, and teleseismic delays, it is anomalous asthenosphere compared to known properties elsewhere. However, this might be expected since it underlies the most negative region of the east—west continental Bouguer gravity profile (latitude 37°) (Fig. 10).

CONCLUSION

Teleseismic residual delays of as much as 1.5 sec, seen on an array of aperture 1,000 km which spanned the region of uplift surrounding the Rio Grande rift, require low velocities to exist deep beneath the crust. Both the block-inversion method and a simple downward projection of the residuals place the low-velocity zone in the depth range 70-100 km, with a velocity contrast of — 8%.

The associated Bouguer gravity variation matches the observations well, given a density contrast of —0.05 gm/cc, adjusted to optimize the fit, i.e., a contrast of 1.6%. A large velocity contrast and small density contrast are indicative of a small fraction of partial melt which, while having a small effect on density, will have a disproportionately larger effect on shear modulus and hence P-wave velocity.

Airy-type isostatic support of the regional uplift through a thickened crust is ruled out in favor of a much deeper low-density zone in the region of the lithosphere—asthenosphere transition.

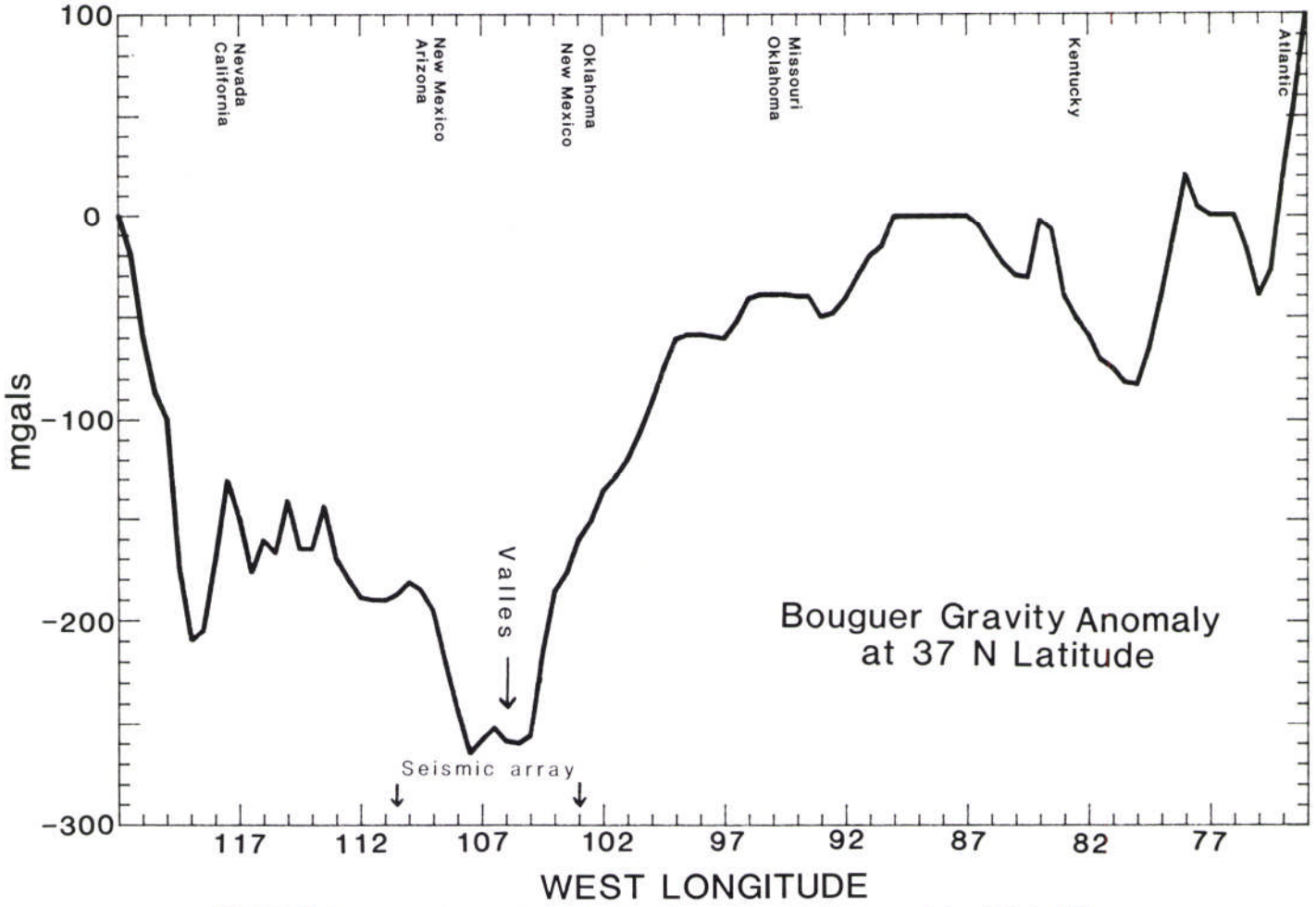

FIGURE 10. Bouguer gravity anomaly for North American continent. Profile measured along latitude 37°N.

ACKNOWLEDGMENT

This work was supported by grants from the Institute of Geophysics and Planetary Physics at Los Alamos and the University of California at Los Angeles.

REFERENCES

Aki, K., 1982, Three-dimensional seismic inhomogeneities in the lithosphere and asthenosphere: evidence for decoupling in the lithosphere and flow in the asthenosphere: Review of Geophysics and Space Physics, 20: 161-170.

__, Christofferson, A., and Huseleye, E. S., 1977, Determination of the three-dimensional seismic structure of the lithosphere: Journal of Geophysical Research, 82: 277-296.

Ander, M. E., 1980, Geophysical study of the crust and upper mantle beneath the central Rio Grande rift and adjacent Great Plains: Ph.D. thesis, University of New Mexico, Albuquerque.

Biswas, N. N., and Knopoff, L., 1974, The structure of the upper mantle under the United States from dispersion of Rayleigh waves: Royal Astronomical Society, Geophysical Journal, 36: 315-450.

Brown, L. D., Krumhansl, P. A., Chapin, C. E., Sanford, A. R., Cook, F. A., Kaufman, S., Oliver, J. E., and Schilt, F. S., 1979, COCORP seismic reflection studies of the Rio Grande rift; *in* Riecker, R. E. (ed.), Rio Grande rift: tectonics and magmatism: American Geophysical Union, Washington, D.C., pp. 169-184.

Burdick, L. J., and Helmberger, D. V., 1978, The upper mantle P-velocity structure of the western United States: Journal of Geophysical Research, 83: 1699-1712.

Christie, P. A. F., and Sclater, J. G., 1980, An extensional origin for the Buchan and Witchgraben in the North Sea: Nature 283: 729-732.

Cordell, L., 1978, Regional geophysical setting of the Rio Grande rift: Geological Society of America, Bulletin, 89: 1073-1090.

Dziewonski, A. M., Hales, A. L., and Lapwood, E. R., 1975, Parametrically simple earth models consistent with geophysical data: Physics of Earth and Planetary Interiors, 10: 12.

Ellsworth, W. A., 1977, Three-dimensional structure of the crust and mantle beneath the island of Hawaii: Ph.D. thesis, Massachusetts Institute of Technology, Cambridge.

Evans, J. R., 1982, Compressional wave velocity structure of the upper 350 km under the Snake River Plain near Rexburg, Idaho: Journal of Geophysics, 87: 2654-4670.

Giese, P. C., Prodehl, C., and Stein, A. (eds.), 1976, Explosion seismology in Central Europe—data and results: Springer-Verlag, New York.

Iyer, H. M., 1975, Anomalous delays of teleseismic P-waves in Yellowstone National Park: Nature, 253: 425-427.

_____ , 1984, Geophysical evidence for the locations, shapes and sizes, and internal structures of magma chambers beneath regions of Quaternary volcanism: Royal Society of London, in press.

_____ , Oppenheimer, D. H., and Hitchock, T., 1979, Abnormal P-wave delays in the Geysers–Clear Lake geothermal area, California: Science, 204: 495-497.

Jenkins, G. M., and Watts, D. G., 1968, Spectral analysis and its applications: Holden–Day, San Francisco.

Keller, G. R., Braile, L. W., and Schlue, J. W., 1979, Regional crustal structure of the Rio Grande rift from surface wave dispersion measurements; *in* Riecker, R. E. (ed.), Rio Grande rift: tectonics and magmatism: American Geophysical Union, Washington. D.C.

Long, R. E., Sundaralingam, K., and Maguire, P. K. H., 1973, Crustal structure of the east African rift zone: Tectonophysics, 20: 269-281.

Murdock, J. N., and Jacksha, L. H., 1981, P-wave velocity of the uppermost mantle of the Rio Grande rift region of north-central New Mexico: Journal of Geophysical Research, 86: 7055-7063.

Oliver, J. E., and Kaufman, S., 1976, Profiling the Rio Grande rift: Geotimes, 27: 20-23.

Olsen, K. H., Keller, G. R., and Stewart, J. N., 1979, Crustal structure along the Rio Grande rift from seismic refraction profiles; *in* Riecker, R. E. (ed.), Rio Grande rift: tectonics and magmatism: American Geophysical Union, Washington, D.C.

Phinney, R. A., 1964, Structure of the Earth's crust from spectral behavior of long-period body waves: Journal of Geophysical Research, 69: 2997-3017.

Priestley, K., and Brune, J., 1978, Surface waves and the structure of the Great Basin: Journal of Geophysical Research, 83: 2265-2272.

_____ , Orcutt, J. A., and Brune, J. N., 1980, Higher-mode surface waves and structure of the Great Basin of Nevada and western Utah: Journal of Geophysical Research, 85: 7166-7174.

Rinehart, E. J., and Sanford, A. R., 1981, Upper crustal structure of the Rio Grande rift near Socorro, New Mexico from inversion of the microearthquake S-wave reflections: Seismological Society of America, Bulletin, 71: 437-450.

__, Sanford, A. R., and Ward, R. M., 1979. Geographic extent and shape of an extensive magma body at midcrustal depths in the Rio Grande rift near Socorro, New Mexico; *in* Riecker, R. E. (ed.), Rio Grande rift: tectonics and magmatism: American Geophysical Union, Washington, D.C., pp. 237-251.

Sanford, A. R., and Long, L. T., 1965, Microearthquake crustal reflections, Socorro, New Mexico: Seismological Society of America, Bulletin, 55: 579-586.

__, Alptekin, 0. S.. and Toppozada, T. R., 1973, Use of reflection phases on microearthquake seismograms to map an unusual discontinuity beneath the Rio Grande rift: Seismological Society of America, Bulletin, 63: 2021-2034.

Sharp, A. D. L., Davis, P. M., and Gray, F., 1980, A low velocity zone below Mount Etna and magma storage: Nature, 287: 587-591.

Spence, W., Gross, R. S., and Jacksha, L. H., 1982, P-wave velocity structure beneath the Jemez lineament, New Mexico: EOS, American Geophysical Union, Transactions, 63 (45): 1117.